Incorporating Intermicellar Interactions in the Fitting of SANS Data from Cationic Wormlike Micelles

Wei-Ren Chen,[†,‡] Paul D. Butler,[‡] and Linda J. Magid*[,†,‡,§]

Department of Chemistry, The University of Tennessee, Knoxville, Tennessee 37996-1600, The NIST Center for Neutron Research, National Institute of Standards and Technology, Gaithersburg, Maryland 20899-8562, and Division of Chemistry, The National Science Foundation, Arlington, Virginia 22230

Received November 11, 2005. In Final Form: May 2, 2006

Small-angle neutron scattering (SANS) from cationic wormlike micellar solutions composed of hexadecyltrimethylammonium bromide (CTABr) and hexadecylpyridinium bromide (CPyBr) in deuterated water was studied at 40 °C as a function of surfactant and salt concentrations. Two scattering functions of semiflexible chains incorporating excluded volume effects, with and without the intermicellar interactions, were used in SANS data model fitting. Two needed changes were made in the well-accepted models. Extensive and systematic SANS data analysis suggests the robustness of these corrected scattering functions when the intermicellar interactions are included. The influence of the headgroups and ionic strength on the contour length and micellar flexibility of these two systems was demonstrated on the basis of the quantitative structural information obtained from the model fitting. Micellar flexibility was found to depend on surfactant concentration, even when intermicellar interactions were taken into account, despite predictions to the contrary.

Introduction

Micellar aggregates are formed through spontaneous self-assembly in aqueous solutions, and the microseparation of the head and tail groups, as a consequence of the hydrophobic effect, gives rise to a rich structural polymorphism.[1] Because of their wide variety of structural and functional roles, micelles are broadly represented in condensed matter science and in biological systems. Moreover, micellar systems are ubiquitous in consumer and industrial applications such as personal-care products, drug-delivery systems, viscosity modifiers in foods and in the processing of polymers, surface modification of materials, and so forth. Microstructural characterization to assess the overall size, chain conformations, and intermicellar interactions over a broad range of fluid compositions is essential to tailoring the macroscopic properties of the complex fluids.[2]

To understand the micellar growth mechanism of ionic surfactant systems in aqueous solvent, it is essential to consider the roles of external control parameters in determining the mesoscopic structure. In general, for a dilute solution above the critical micelle concentration (cmc), the preferred self-assembled geometry is spherical. By tuning the experimental conditions, such as changing the temperature, increasing the surfactant concentration, or varying the salinity, one can trigger a structural evolution of micellar aggregates toward nonspherical elongated shapes. The further the change, the more energetically favorable it becomes for micelles to grow uniaxially away from the spherical micelles into large anisotropic aggregates such as cylindrical micelles. Under proper experimental conditions, the micelles can grow to several micrometers along their axes.

To understand micellar growth quantitatively, a theory based on the Flory−Huggins approach was proposed to give the distribution of the charged wormlike micelles in the semidilute regime and in the presence of a salt.[3] In terms of the average micellar contour length, $\langle L \rangle$, this is expressed as

$$\langle L \rangle \alpha \phi^{1/2} \tag{1}$$

where ϕ is the effective volume fraction and

$$N(L) \approx \exp\left(\frac{L}{\langle L \rangle}\right) \tag{2}$$

where $N(L)$ is the number of chains of length L. Several studies indeed suggest its validity despite its mean-field nature.[4]

The intrinsic flexibility of the wormlike micellar chain, characterized by Kuhn length, primarily depends on the chemical details of the surfactant monomer. The theory proposed by Odijk, Skolnick, and Fixman (OSF) first shows that the total persistence length is given by the sum of the intrinsic rigidity and an additional contribution due to the electrostatic repulsion of like charges on the micellar surface.[5,6] Recently, a theoretical prediction based on variational calculations indicated that the scaling of the electrostatic persistence length is far more complex than the OSF prediction and depends on the relative value of the intrinsic rigidity as well.[7]

Small-angle neutron scattering (SANS) can be used to obtain structural information. Obtaining quantitative micellar structural information requires accurate scattering data analysis based on the model scattering function. In 1996, Pedersen and Schurtenberger[8] provided a parametrized scattering function for semiflexible chains without intermicellar interactions. It was found to be a robust model for dilute systems. In 1999, they further proposed a model to incorporate the intermicellar interactions.[9] Two different schemes, RPA and PRISM, were developed

* Corresponding author. E-mail: lmagid@nsf.gov.
† The University of Tennessee.
‡ National Institute of Standards and Technology.
§ The National Science Foundation.

(1) Israelachvili, J. N. *Intermolecular and Surface Forces*, 2nd ed.; Academic Press: New York, 1992.
(2) Magid, L. J. *J. Chem. Phys. B* **1998**, *102*, 4064.
(3) Cates, M. E.; Candau, S. J. *J. Phys.: Condens. Matter* **1990**, *2*, 6869.
(4) Svaneborg, C.; Pedersen, J. S. *Curr. Opin. Colloid Interface Sci.* **2004**, *8*, 507.
(5) Skolnick, J.; Fixman, M. *Macromolecules* **1977**, *10*, 944.
(6) Odijk, T. *J. Polym. Sci., Polym. Phys. Ed.* **1977**, *15*, 477.
(7) Ha, B. Y.; Thirumala, D. *J. Chem. Phys.* **1999**, *110*, 7533.
(8) Pedersen, J. S.; Schurtenberger, P. *Macromolecules* **1996**, *29*, 7602.
(9) Pedersen, J. S.; Schurtenberger, P. *Europhys. Lett.* **1999**, *45*, 666.

10.1021/la0530440 CCC: $33.50
Published on Web 06/17/2006

subsequently to implement the fitting of scattering data from wormlike chains, and both have been widely used since then.[10−15] To avoid the breakdown observed at large concentrations and large Q values when the RPA approximation was used for the model fitting, in our work, the PRISM approach was used to incorporate intermicellar interactions. Prior to our work, both PRISM and RPA model fittings use fixed micellar rigidity as an input, and even with that constraint, agreement between fitted and experimental curves was often poor. To our knowledge, so far there is no report of success in allowing wormlike micellar rigidity to be optimized in any model fitting incorporating intermicellar interactions.

We discovered and corrected two unphysical errors, in the low-Q and crossover regions where two asymptotic functional forms meet, in the scattering function without interchain interactions. Two different schemes incorporating the intermicellar interactions based on this modified single-chain model as the reference system—either Kuhn length b, a length scale characterizing the micellar rigidity, is fixed to an extrapolated value or treated as a fitting parameter—were used in our study. Moreover, we propose a different protocol to implement the PRISM model fitting by obtaining the interaction parameter, which is essential for PRISM fitting, in a different way. Comprehensive SANS data analysis proves the ability of the new model to include the intermicellar interactions reliably. We illustrate this by analyzing the impact of surfactant headgroups and salt concentration on overall micellar contour lengths and flexibility based on the new model.

The present study is organized as follows. We first discuss the scattering functions of wormlike chains, with or without the inclusion of intermicellar interactions, followed by the methodology of different model fittings in Materials and Methods.

In Results and Discussion, the results of SANS measurements deduced from different model fittings are presented and discussed in the following sequence. The single-chain model fittings are presented first. Special emphasis will be given to the effects of headgroup and ionic strength on the micellar structure. Then a comparison of two schemes, b fixed and b varying, to implement PRISM fitting, using PRISM protocol 1 (Materials and Methods), is presented and discussed. Finally, we demonstrate and discuss the results obtained from protocols 1 and 2 of the PRISM fittings.

We summarize this report in Conclusions, and the modifications of the scattering function without intermicellar interactions are detailed in the Appendix and Supporting Information.

Materials and Methods

Materials. Hexadecyltrimethylammonium chloride (CTACl) and hexadecylpyridinium chloride monohydrate (CPyCl, >98% purity) were obtained from Fluka and used without further purification. Sodium bromide (NaBr, >99% purity) came from Sigma-Aldrich. Deuterium oxide (D_2O, >99.9% purity) was obtained from Cambridge Isotope Laboratories, Inc. Samples with surfactant concentrations ranging from 1 to 10 mM in NaBr aqueous solutions were prepared with concentrations of 0.25, 0.5, 0.8, and 1.0 M NaBr.[16]

Small-Angle Neutron Scattering (SANS). SANS measurements were performed on the NG-7 SANS instrument at the NIST Center for Neutron Research. Incident neutron wavelengths of 6.0 and 9.0 Å, with a wavelength spread $\Delta\lambda/\lambda$ of 10%, resulted in scattering wave vectors Q ranging from 0.002 to 0.12 $Å^{-1}$. The samples were contained in quartz cells with path lengths ranging from 1 to 5 mm, and all the experiments were performed at a controlled temperature of 40.0 °C ± 0.1 °C. Backgrounds from the different NaBr solutions were measured and used for corrections instead of using pure D_2O. The measured intensity was also corrected for detector background and sensitivity and for scattering from empty cell contributions and was normalized to a reference scattering intensity of a polymer sample with a precisely known cross section.

Analysis of SANS Intensity Distributions. *Single-Chain Model.* SANS provides a powerful tool for obtaining quantitative information about wormlike micelles. The Q variation of the SANS intensity distribution $I(Q)$ of a general wormlike chain is characterized by several asymptotic regions that contain information about different characteristic lengths in real space: In the very small Q region, the decay of $I(Q)$ follows the Guinier law (i.e., $I(Q) \sim (1 - (Q^2R_G^2/3))$ allowing the determination of the radius of gyration R_G or, equivalently, the contour length L ($\langle R_G^2\rangle \approx (bL/6)$). As Q increases, $I(Q)$ is governed by a power law decay as the result of chain flexibility and parametrized by the Kuhn length. At higher Q, a characteristic power law of the form $I(Q) \approx Q^{-1}$ is observed, indicating that wormlike micelles resemble long, thin rods on this length scale. This region is followed by a further decay of $I(Q)$ that contains information regarding the micellar radial cross section. If the theoretical scattering function, with Q, L, and b as parameters, is available, then quantitative structural information can be extracted by performing model fitting on the full-range scattering curve.

In the past few decades, the structure of the real wormlike chain has attracted considerable attention.[2,4,17] Evolving from the Debye function, which is the scattering function of the Gaussian chain, several theoretical studies have been made to model the scattering function of a realistic wormlike chain. Details can be found in an excellent review article by Schurtenberger.[17] One insurmountable limitation for real wormlike chain modeling is the mathematical complexity of taking into account excluded volume effects. Because of this constraint, the scattering function of real wormlike chains still remains unknown analytically.

Another approach to obtaining quantitative micellar structural information is based on Monte Carlo simulations of the Kratky and Porod wormlike chain models. Pedersen and Schurtenberger incorporated the excluded volume effect into a parametrized wormlike chain model[8] and proposed a phenomenological expression of a full scattering function of semiflexible chains $S_{WC}(Q, L, b)$ with an excluded volume effect. This approach necessitates the crossover functions, determined by fitting the results generated from Monte Carlo simulations, to connect scattering functions with two asymptotic regions and to correct that crossover region.

If the contour length of the chains is significantly larger than the cross-sectional radius, then the scattering from the cross section can be separated from the contour length and the Kuhn length. Therefore, the total scattering function of a wormlike chain can be obtained from the decoupling approximation[18] as

$$I_{WC}(Q, L, b, R_{CS}) = c\Delta\rho_m{}^2 M S_{WC}(Q, L, b)\, P_{CS}(Q, R_{CS}) \quad (3)$$

where c is the surfactant concentration, M gives the average molecular weight of the micelles, and $S_{WC}(Q, L, b)$ is the scattering function of single semiflexible chain with excluded volume effects as proposed in Method 3 of ref 8. The scattering function from the cross section of a rigid rod is given by

$$P_{CS}(Q, R_{CS}) = \left[\frac{2J_1(QR_{CS})}{QR_{CS}}\right]^2 \quad (4)$$

where $J_1(x)$ denotes the Bessel function of the first kind.

(10) Bombelli, F. B.; Berti, D.; Pini, F.; Keiderling, U.; Baglioni, P. *J. Chem. Phys. B* **2004**, *108*, 16427.
(11) Garamus, V. M.; Pedersen, J. S.; Kawasaki, H.; Maeda, H. *Langmuir* **2000**, *16*, 6431.
(12) Arleth, L.; Bergström, M.; Pedersen, J. S. *Langmuir* **2002**, *18*, 5343.
(13) Ericsson, C. A.; Söderman, O.; Garamus, V. M.; Bergström, M.; Ulvenlund, S. *Langmuir* **2005**, 21, 1507.
(14) Garamus, V. M.; Pedersen, J. S.; Maeda, H.; Schurtenberger, P. *Langmuir* **2003**, *19*, 3656.
(15) Arleth, L.; Bauer, R.; Ogendal, L. H.; Egelhaaf, S. U.; Schurtenberger, P.; Pedersen, J. S. *Langmuir* **2003**, *19*, 4096.

(16) In its own activities as a scientific institution, NIST uses many different materials, products, types of equipment, and services. However, NIST does not approve, recommend, or endorse any product or proprietary material.

The polydispersity of the contour length is incorporated by means of a Schulz−Zimm distribution for polydispersity index z fixed at 1 (hence $M_w/M_n = 2$), as suggested by the ladder model[19]

$$\langle S_{WC}(Q, L, b)\rangle_{SZ} = \frac{\int N_{SZ}(L)L^2 S_{WC}(Q, L, b)\, dL}{\int N_{SZ}(L)L^2\, dL} \quad (5)$$

where

$$N_{SZ}(L) = \frac{L^z}{z!}\left(\frac{z+1}{\langle L\rangle}\right)^{(z+1)} \exp\left[\frac{-L(z+1)}{\langle L\rangle}\right] \quad (6)$$

Therefore, the scattering function of the wormlike micellar system in the *absence* of intermicellar interactions is given by[18]

$$\langle I_{WC}(Q, L, b, R_{CS})\rangle_{SZ} = c\Delta\rho_m{}^2 M\langle S_{WC}(Q, L, b)\rangle_{SZ} P_{CS}(Q, R_{CS}) + BD \quad (7)$$

with *BD* denoting the residual scattering from the solvent and incoherent background.

Many-Chain Systems − PRISM Protocol 1. Several scattering experiments and Monte Carlo simulations suggest[9,12,20] that in order to obtain the correct micellar structural information it is essential to incorporate intermicellar interactions into the single-chain model.

On the basis of the polymer reference interaction site model (PRISM)[21] and Monte Carlo simulations, Pedersen and Schurtenberger proposed a new structure factor to interpret the influence of concentration on the static structure of wormlike chains on all length scales[9]

$$S_{PRISM}(Q, L, b) = \frac{S_{WC}(Q, L, b)}{1 + \beta c(Q)\, S_{WC}(Q, L, b)} \quad (8)$$

where β is a parameter characterizing the strength of the intermicellar interaction. $c(Q)$ is the normalized Fourier transform of the direct correlation function for spheres on the chain and is found empirically to be approximately the form factor of an infinitely thin rod. The PRISM approach to obtaining the structure factor of interacting wormlike chains is based on solving the Ornstein−Zernike integral equation of micellar liquids interacting via a specific intermicellar potential, with a proper closure relation. The incorporation of the intermicellar interaction into the ideal noninteracting wormlike micelles is treated as a weak perturbation for the reference system.[22]

Similar to eq 7, the scattering function of the wormlike micellar system with intermicellar interactions can be written as

$$\langle I_{WC}(Q, L, b, R_{CS})\rangle_{SZ} = c\Delta\rho_m{}^2 M_w\langle S_{PRISM}(Q, L, b)\rangle_{SZ} P_{CS}(Q, R_{CS}) + BD \quad (9)$$

Here we follow the procedure proposed in ref 18 to incorporate the effect of the polydispersity of different wormlike micelles. Implementing the PRISM model fitting requires the interaction parameter β as an input in advance. It can be expressed explicitly in terms of $S(0)$, the structure factor at zero angle containing information about the interaction among the constitution components of the system, as

$$\beta = \frac{1 - S(0)}{S(0)} \quad (10)$$

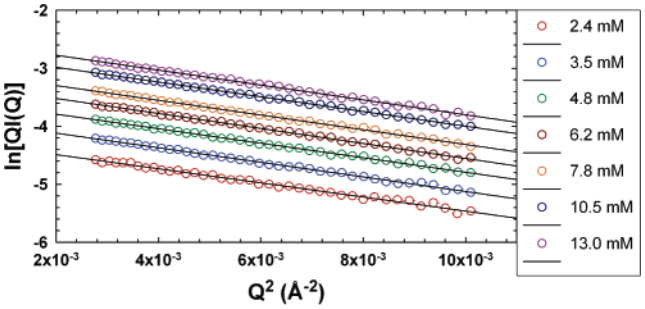

Figure 1. Guinier-like plot of the SANS data in the intermediate-Q region for CPyBr of various concentrations in 0.25 M NaBr. Solid lines show the fits according to eqs 13 and 14.

Renormalization group theory (RGT)[23] calculations show that $S(0)$ can further be expressed in terms of concentration c. The detailed fitting protocol was provided by Schurtenberger and co-workers and can be found in refs 10−13.

Weighted nonlinear least-squares fitting with a grid-search method was used to perform the PRISM model fitting. Two different schemes were used to take into account the local flexibility: either b is fixed to $b_{c=0}$, obtained from the fitting results with single-chain model, or b is treated as a fitting parameter. The results obtained from these two approaches are compared in Results and Discussion.

Many-Chain Systems − PRISM Protocol 2. Alternatively, we propose another protocol for obtaining the $S(0)$ needed for the PRISM fitting. It is known that $S(0)^{-1}$ can be determined from the SANS forward-scattered intensity by

$$I(Q \to 0) = c\Delta\rho_m{}^2 M_{app} = c\Delta\rho_m{}^2 M_w S(0) \quad (11)$$

where M_w can be expressed as

$$M_w = M_S L\left(\frac{z+2}{z+1}\right)\left\langle\frac{N}{L}\right\rangle_w \quad (12)$$

with M_S being the molecular weight of the surfactant.

Following an argument first proposed by Porod,[19,24,25] local structural information such as the weight-average aggregation number per unit length and the micellar cross section can be determined through a Guinier-like plot, namely, a plot of $QI(Q)$ versus Q^2, in the intermediate-to-high Q region. As mentioned in the previous section, the fair separation of length scales of the aggregates allows one to extract information about the local structure in the Q range of 2×10^{-3}Å$^{-2} < Q^2 < 10^{-2}$Å^{-2}. The explicit mathematical expression of the equation is

$$QI(Q) = K \exp(-Q^2 R_{G,CS}{}^2) \quad (13)$$

For a circular cross section, the micellar radius is

$$R_{CS} = \sqrt{2} R_{G,CS}$$

The value of K is given by

$$K = c\tau\left\langle\frac{N}{L}\right\rangle_w (b_m - V_m\rho_s)^2 \quad (14)$$

where b_m and V_m are the sum of the neutron scattering lengths and the volume per surfactant monomer in the micelle, respectively, and ρ_s is the scattering length density of the solvent. $\langle N/L\rangle_w$ is the weight-average aggregation number per unit length, and $R_{G,CS}$ is the weight-average radius of gyration of the cross section of the cylinder, b_m and V_m are the sum of the neutron scattering lengths and the volume

(17) Schurtenberger, P. In *Neutrons, X-rays and Light: Scattering Methods Applied to Soft Condensed Matter*; Lindner, P., Zemb, Th., Ed.; North-Holland: Amsterdam, 2002.
(18) Jerke, G.; Pedersen, J. S.; Egelhaaf, S. U.; Schurtenberger, P. *Phys. Rev. E* **1997**, *56*, 5772.
(19) Schmidt, M.; Paradossi, G.; Burchard, W. *Makromol. Chem. Rapid Commun.* **1985**, *6*, 767.
(20) Bombelli, F. B.; Berti, D.; Keiderling, U.; Baglioni, P. *J. Chem. Phys. B* **2002**, *106*, 11613.
(21) Schweizer, K. S.; Curro, J. G. *Adv. Polym. Sci.* **1994**, *116*, 319.
(22) Hansen, J. P.; McDonald, I. R. *Theory of Simple Liquids*, 2nd ed.; Academic Press: London, 1986.
(23) Ohta, T.; Oono, Y. *Phys. Lett.* **1982**, *89A*, 460.
(24) Casassa, E. F. *J. Chem. Phys.* **1955**, *23*, 596.
(25) Holtzer, A. *J. Polym. Sci.* **1955**, *17*, 433.

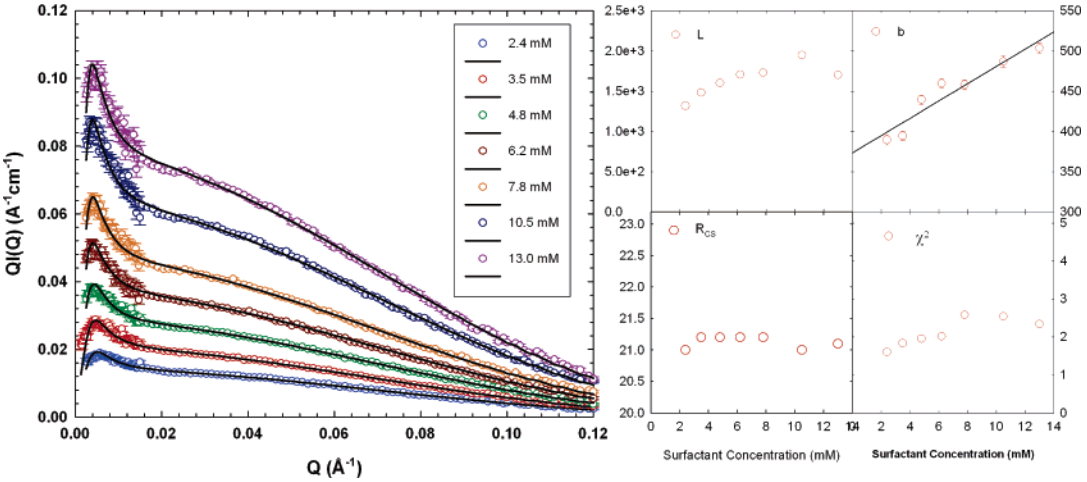

Figure 2. SANS intensity distributions and the associated bending rod plots for CPyBr in 0.25 M NaBr at 40 °C. The solid curves give the corresponding single-chain model fits using eqs 7 and 17. The concentration dependences of the fitted parameters and of χ^2 are given in the bottom panels.

per surfactant monomer in the micelle, respectively, with ($b_m - V_m\rho_s$) being the contrast.

Upon substituting eqs 12 and 14 into eq 10, it is found that

$$\beta = \frac{M_S}{M_{app}} L\left(\frac{z+2}{z+1}\right)\left[\frac{K}{\pi c(b_m - V_m\rho_s)^2}\right] - 1 \qquad (15)$$

allowing eq 8 to be rewritten as

$$S_{PRISM}(Q, L, b) = \frac{S_{WC}(Q, L, b)}{1 + \left\{\frac{M_S}{M_{app}} L\left(\frac{z+2}{z+1}\right)\left[\frac{K}{\pi c(b_m - V_m\rho_s)^2}\right] - 1\right\} c(Q)\, S_{WC}(Q, L, b)} \qquad (16)$$

The advantage of this approach is that $S(0)^{-1}$ can be determined directly from the analysis of the forward scattering without using the complicated mathematical expressions given by RGT. A comparison of PRISM model fittings with these two protocols is given in Results and Discussion.

Upon increasing the surfactant concentration or varying the salinity, the growth of wormlike micelles with very large values of the contour length may occur. The result is a very sharp upturn in the low-Q part of the SANS scattering intensity distributions. To obtain accurate estimates of the contour length from the model fitting, it is essential to take a resolution correction into account. This was accomplished by integrating the theoretical scattering intensity obtained from the theoretical models with a Gaussian resolution function

$$I(Q) = \int_{Q_{MIN}}^{Q_{MAX}} \frac{\langle I_{WC}(y, L, b, R_{CS})\rangle_{SZ}}{\sqrt{2\pi\sigma_R^2}} \exp\left[-\frac{(Q-y)^2}{2\sigma_R^2}\right] dy + BD \qquad (17)$$

where σ_R is the full width at half-height of the resolution function of the instrument. We then used this ''smeared" intensity distribution to fit the SANS intensity distributions.

Results and Discussion

Local Micellar Structure. The average aggregation number per unit length can be deduced by using eqs 13 and 14. As an example, the Guinier-like plots of SANS intensity distributions obtained from CPyBr of various concentrations in 0.25 M NaBr solutions are reported in Figure 1. For CPyBr micelles, the value of $\langle N/L\rangle_w$ obtained from the fitting is about 1.7 Å^{-1}, and that for CTABr, about 2.1 Å^{-1}. In principle, $\langle N/L\rangle_w$ is not dependent on surfactant concentration c.

Fitting of the Full Scattering Curves − Single-Chain Model. The SANS intensity distributions were first fit using eqs 7 and 17, that is, without taking the intermicellar interactions into account. Two series of scattering curves are illustrated in bending rod plots as a demonstration: Figure 2 shows the fits to the scattering curves for CPyBr in 0.25 M NaBr, and Figure 3, for CTABr in 0.25 M NaBr. It is evident that the agreement with experimental data is indeed satisfactory within the whole surfactant concentration range studied.

Table 1 reports the fitting parameters obtained from the single-chain model fitting. Several important points need to be addressed. As demonstrated by Schurtenberger et al,[17,18,26−28] the analysis of the bond angle correlation function provided by Monte Carlo simulation suggests that once interactions are taken into account the Kuhn length b should not change with concentration. From this perspective, the unphysical but evident concentration dependence of b is not a result of real intrinsic stiffening of the wormlike micelles and should be ascribed to the neglect of intermicellar interactions in the fitting. Figures 4 and 5 give the extracted Kuhn length b as a function of surfactant concentration c at various NaBr concentrations for CPyBr and CTABr, respectively. Linear trends are observed for all studied samples. Both Figures show that, as suggested by the intercepts at c = 0, the micellar flexibility increases as the salt concentration increases. This is due to the fact that the Coulomb interaction among the neighboring molecules in the aggregates is screened by the addition of salt. Figure 5 suggests that, for all of the CTABr concentrations studied in this research, the intramicellar electrostatic interaction is completely screened when the concentration of NaBr is higher than 0.5 M. In other words, the Kuhn length b obtained from the model fitting at such high salt concentrations can be considered to be the intrinsic rigidity. A comparison of the apparent dependence of the fitted Kuhn length b on surfactant concentrations for two different wormlike micellar systems is presented in Figure 6. The infinite dilution extrapolated values clearly show that at the same NaBr concentration the pyridinium headgroups confer greater flexibility. This is probably because of their planar head structure, whereas the geometry at the N in the trimethylammonium headgroup is tetrahedral.

(26) Cannavacciuolo, L.; Sommer, C.; Pedersen, J. S.; Schurtenberger, P. *Phys. Rev. E* **2000**, *62*, 5409.
(27) Cannavacciuolo, L.; Pedersen, J. S.; Schurtenberger, P. *J. Phys.: Condens. Matter* **2002**, *14*, 2283.
(28) Cannavacciuolo, L.; Pedersen, J. S.; Schurtenberger, P. *Langmuir* **2002**, *18*, 2922.

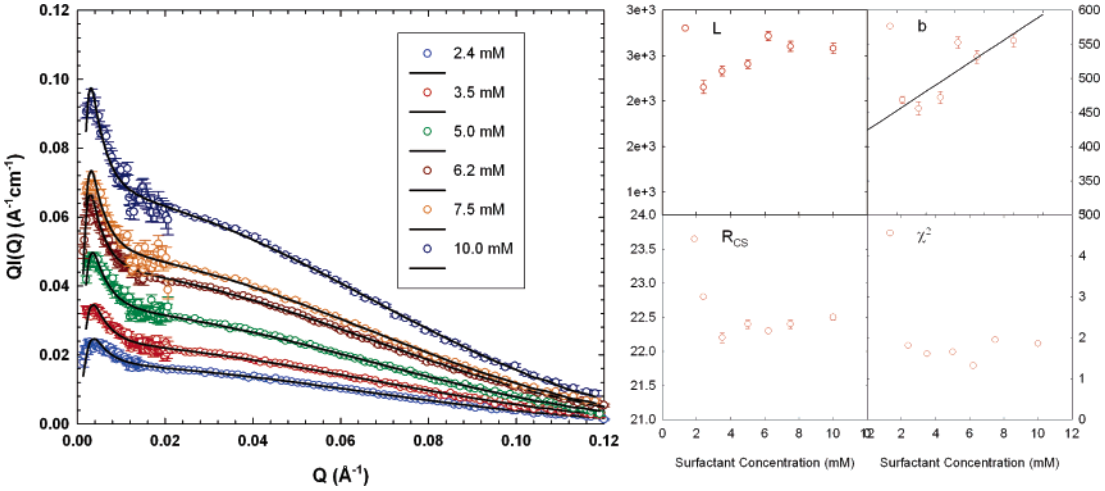

Figure 3. SANS intensity distributions and the associated bending rod plots for CTABr in 0.25 M NaBr at 40 °C. The solid curves give the corresponding single-chain model fits using eqs 7 and 17. The concentration dependences of the fitted parameters and of χ^2 are given in the bottom panels.

Table 1. Fitted Parameters for Micelles with the Single-Chain Model

c(mM)	L(Å)	b(Å)	R_{CS}(Å)	c(mM)	L(Å)	b(Å)	R_{CS}(Å)
			CPyBr Micelles in 0.25 M NaBr				
2.4	1315.0 ± 1.6%	389.2 ± 1.6%	21.0 ± 0.3%	7.8	1726.5 ± 1.4%	457.8 ± 1.3%	21.2 ± 0.2%
3.5	1478.8 ± 1.5%	394.2 ± 1.4%	21.2 ± 0.2%	10.5	1946.1 ± 1.9%	486.5 ± 1.4%	21.0 ± 0.1%
4.8	1598.0 ± 1.4%	439.4 ± 1.3%	21.2 ± 0.2%	13.0	1697.8 ± 1.4%	503.3 ± 1.3%	21.1 ± 0.1%
6.2	1705.5 ± 1.5%	459.4 ± 1.3%	21.2 ± 0.2%				
			CPyBr Micelles in 0.5 M NaBr				
2.6	2649.7 ± 1.5%	334.5 ± 1.2%	21.2 ± 0.4%	6.2	3581.6 ± 1.6%	392.3 ± 1.0%	21.5 ± 0.3%
3.8	3270.9 ± 1.6%	346.5 ± 1.1%	21.2 ± 0.3%	7.8	3581.0 ± 1.7%	420.0 ± 1.0%	21.5 ± 0.2%
4.8	3364.2 ± 1.5%	354.2 ± 1.0%	21.3 ± 0.3%	10.0	3511.3 ± 1.5%	418.6 ± 1.0%	21.6 ± 0.2%
			CPyBr Micelles in 0.8 M NaBr				
1.04	2064.0 ± 1.1%	252.8 ± 1.1%	19.2 ± 0.5%	2.5	3231.2 ± 1.9%	323.1 ± 1.2%	21.5 ± 0.4%
1.28	1912.6 ± 1.1%	266.4 ± 1.0%	19.2 ± 0.4%	3.1	4302.5 ± 2.0%	331.8 ± 1.1%	21.4 ± 0.3%
1.52	2127.9 ± 1.1%	269.1 ± 1.0%	19.6 ± 0.4%	3.12	3246.2 ± 1.2%	336.0 ± 0.7%	20.5 ± 0.2%
1.92	2416.6 ± 1.1%	285.1 ± 0.8%	19.9 ± 0.3%	4.0	3416.4 ± 2.1%	341.6 ± 1.1%	21.6 ± 0.3%
			CTABr Micelles in 0.15 M NaBr				
2.0	835.5 ± 1.9%	955.7 ± 67.8%	21.3 ± 0.3%	5.0	1022.1 ± 1.3%	727.6 ± 2.5%	22.0 ± 0.2%
3.5	1019.1 ± 1.6%	1151.8 ± 44.0%	21.8 ± 0.2%	7.5	1095.2 ± 1.2%	618.9 ± 1.7%	21.9 ± 0.2%
			CTABr Micelles in 0.25 M NaBr				
2.4	2152.5 ± 3.3%	468.5 ± 1.1%	22.8 ± 0.1%	6.2	2715.3 ± 1.9%	552.5 ± 1.5%	22.3 ± 0.2%
3.5	2330.7 ± 2.3%	456.1 ± 2.1%	22.2 ± 0.4%	7.5	2601.1 ± 2.2%	531.3 ± 1.8%	22.4 ± 0.3%
5.0	2405.1 ± 2.0%	472.0 ± 1.8%	22.4 ± 0.3%	10.0	2579.2 ± 2.2%	555.5 ± 1.8%	22.5 ± 0.2%
			CTABr Micelles in 0.5 M NaBr				
1.4	2788.6 ± 1.2%	338.9 ± 0.7%	21.0 ± 0.3%	3.2	3166.2 ± 2.2%	400.2 ± 0.8%	21.5 ± 0.2%
2.0	3034.5 ± 2.0%	370.1 ± 0.8%	21.5 ± 0.3%	3.8	3658.1 ± 2.6%	409.2 ± 0.7%	21.6 ± 0.2%
2.6	3498.9 ± 2.0%	361.7 ± 0.7%	21.3 ± 0.2%	4.4	3662.2 ± 2.7%	407.9 ± 0.7%	21.7 ± 0.2%
			CTABr Micelles in 1.0 M NaBr				
1.3	3902.9 ± 3.5%	359.0 ± 2.1%	22.8 ± 0.4%	2.6	5415.8 ± 4.0%	431.7 ± 1.8%	22.5 ± 0.3%
1.7	6129.5 ± 4.6%	341.1 ± 1.4%	22.7 ± 0.4%	3.2	6859.6 ± 3.5%	405.9 ± 1.3%	22.5 ± 0.3%
2.0	5112.9 ± 3.3%	403.1 ± 1.7%	22.4 ± 0.3%	3.8	7081.4 ± 3.6%	423.6 ± 1.3%	22.5 ± 0.3%
2.3	5008.2 ± 3.2%	393.0 ± 1.6%	22.6 ± 0.3%				

Moreover, Table 1 shows that the CPyBr micelles have smaller radii, which may be due to the difference in packing of the hydrocarbon chains near the headgroup (i.e., there are more gauche conformations in the pyridinium cases).

Fitting of the Full Scattering Curves − PRISM Protocol 1. As already stressed, the consensus in the literature is that the inclusion of the intermicellar interaction is essential to the correction of the apparent dependence of micellar flexibility on surfactant concentration. To take the interactions into consideration, eqs 9 and 17 were used to fit the SANS intensity distributions. As suggested by Schurtenberger and co-workers,[18] our first scheme using PRISM involved setting b equal to the $c = 0$ extrapolated value at each surfactant concentration. The micellar cross-sectional radii and background term were also fixed during the fitting.

Results are found in Table 2, and an example of CPyBr in 0.25 M NaBr is given in Figure 7a. Compared with the single-chain model fitting (given as the green symbol in the insets), PRISM fitting with the fixed flexibility approximation (blue symbols) gives a weaker dependence of L on c. In general, the model fitting gives a qualitatively reasonable description of the intermicellar interaction that is characterized by the parameter $S(0)$. However, as the surfactant concentration increases, the disagreement between the experimental data points and the model curves is more noticeable, especially around the low-Q and crossover regions. The disagreement is found for the entire series

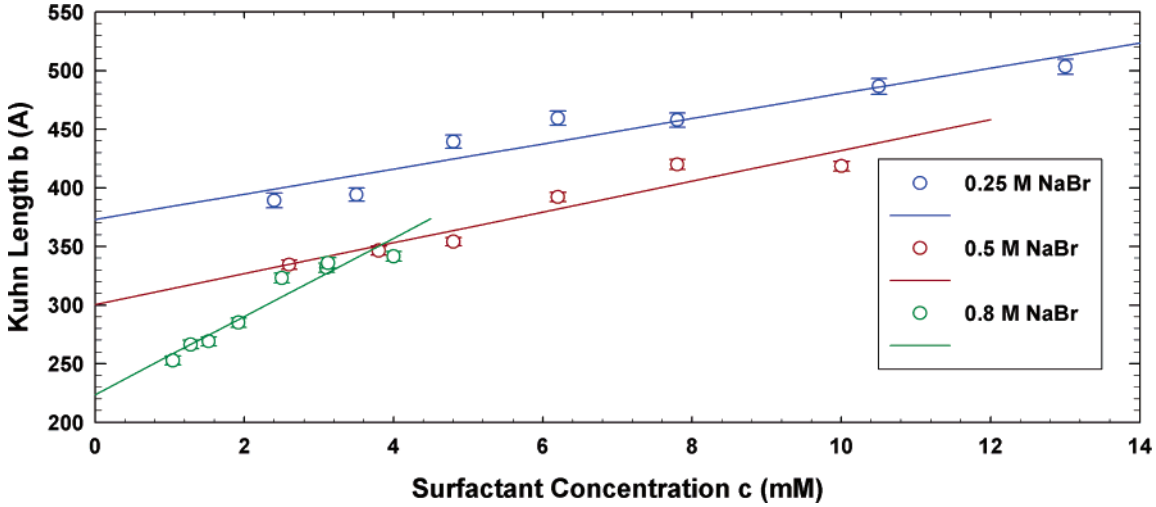

Figure 4. Dependence of the fitted Kuhn lengths on CPyBr surfactant concentration at three NaBr concentrations.

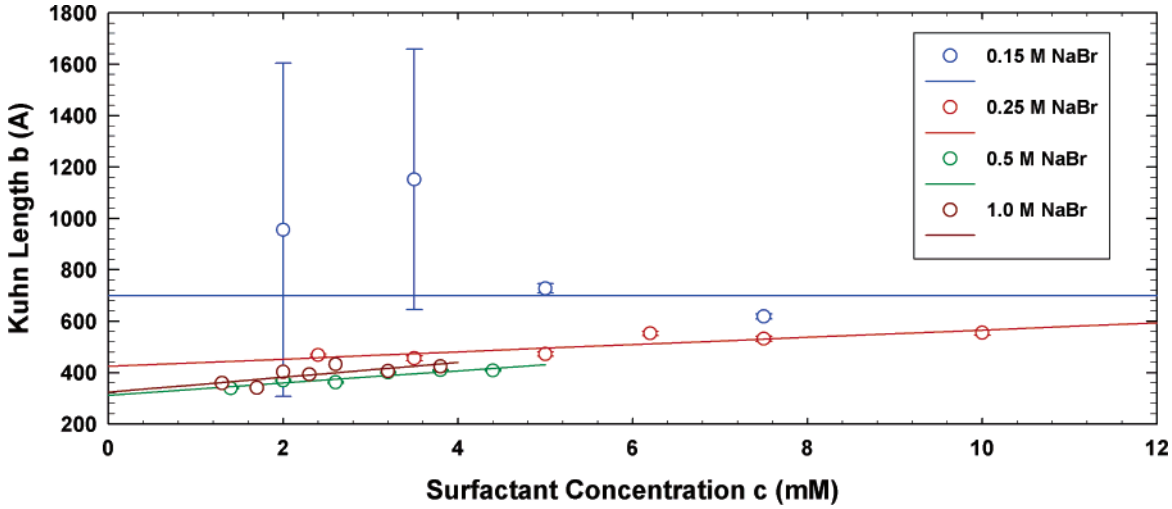

Figure 5. Dependence of the fitted Kuhn lengths on CTABr surfactant concentration at four NaBr concentrations.

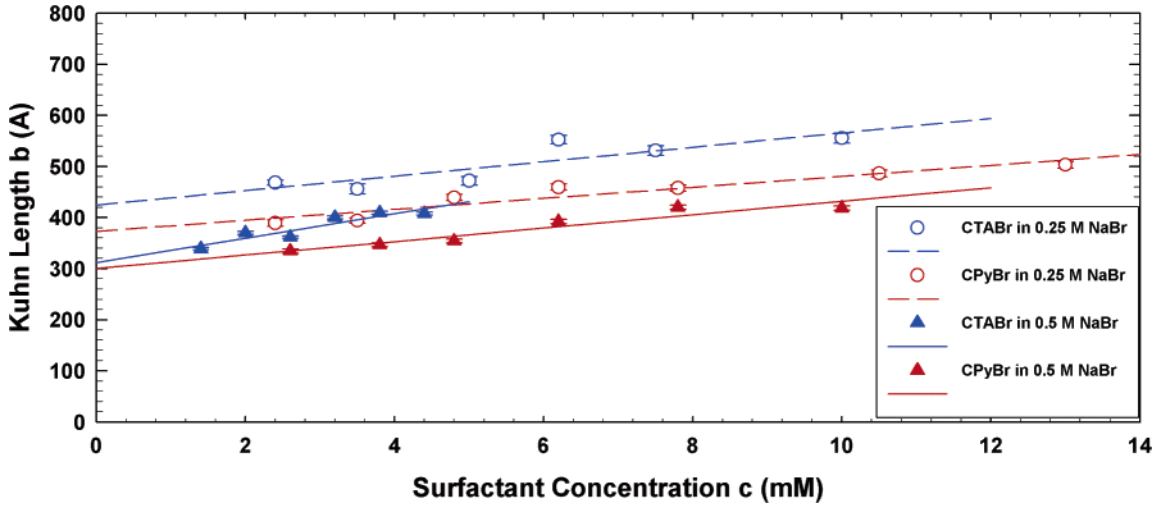

Figure 6. Dependence of the fitted Kuhn lengths on two different headgroups.

of fitted SANS curves represented in Table 2 for samples with high surfactant concentrations.

It is our discovery that in general the inclusion of *b* as a fitting parameter significantly improves the quality of the fits. The experimental bending rod plots and their associated fitting curves are given in Figure 7b. Complete fitted parameters are tabulated in Table 3. A comparison of the final χ^2 presented in the insets of the bottom panel demonstrates that this new approach (red symbols) indeed gives a better description of the experimental curves. However, it is evidently in contradiction with the

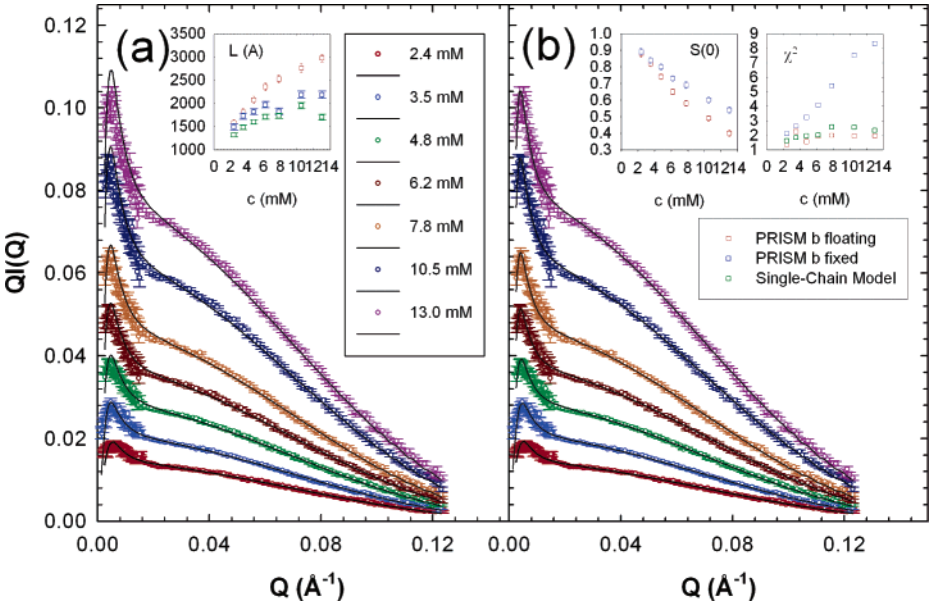

Figure 7. Comparison of fitting results presented in bending rod plots of the two different PRISM schemes, with fixed (panel a) and floating (panel b) Kuhn lengths.

Table 2. Fitted Parameters for Micelles in NaBr with the PRISM Model with Fixed *b*

c(mM)	*L*(Å)	*b*(Å)	R_{CS}(Å)	*S*(0)	*c*(mM)	*L*(Å)	*b*(Å)	R_{CS}(Å)	*S*(0)
CPyBr Micelles in 0.25 M NaBr									
2.4	1492.4 ± 1.7%	373.1	21.0 ± 0.3%	0.89	7.8	1824.6 ± 1.3%	373.1	21.2 ± 0.2%	0.69
3.5	1720.3 ± 1.7%	373.1	21.2 ± 0.2%	0.84	10.5	2185.0 ± 1.3%	373.1	21.0 ± 0.1%	0.60
4.8	1810.4 ± 1.4%	373.1	21.2 ± 0.2%	0.80	13.0	2180.8 ± 1.2%	373.1	21.1 ± 0.1%	0.54
6.2	1970.0 ± 1.4%	373.1	21.2 ± 0.2%	0.73					
CPyBr Micelles in 0.5 M NaBr									
2.6	2682.5 ± 1.3%	300.6	21.2 ± 0.4%	0.87	6.2	3851.2 ± 1.1%	300.6	21.5 ± 0.3%	0.68
3.8	3567.1 ± 1.3%	300.6	21.4 ± 0.3%	0.79	7.8	3898.2 ± 1.1%	300.6	21.5 ± 0.2%	0.62
4.8	3694.7 ± 1.2%	300.6	21.3 ± 0.3%	0.74	10.0	4054.3 ± 1.0%	300.6	21.6 ± 0.2%	0.55
CPyBr Micelles in 0.8 M NaBr									
1.04	2003.5 ± 0.9%	223.8	19.2 ± 0.5%	0.97	2.5	2777.5 ± 1.5%	223.8	21.4 ± 0.4%	0.91
1.28	1802.6 ± 0.9%	223.8	19.2 ± 0.4%	0.97	3.1	2874.3 ± 1.5%	223.8	21.4 ± 0.3%	0.89
1.52	1969.5 ± 0.8%	223.8	19.6 ± 0.4%	0.96	3.12	2376.6 ± 0.8%	223.8	20.5 ± 0.2%	0.83
1.92	2321.3 ± 0.7%	223.8	19.9 ± 0.3%	0.94	4.0	2954.6 ± 1.5%	223.8	21.6 ± 0.3%	0.86
CTABr Micelles in 0.15 M NaBr									
2.0	857.3 ± 1.1%	700.0	21.3 ± 0.3%	0.87	5.0	1353.0 ± 1.1%	700.0	22.0 ± 0.2%	0.68
3.5	1092.8 ± 1.0%	700.0	21.8 ± 0.2%	0.76	7.5	1802.9 ± 1.2%	700.0	21.9 ± 0.2%	0.53
CTABr Micelles in 0.25 M NaBr									
2.4	2180.7 ± 1.9%	424.6	22.8 ± 0.1%	0.90	6.2	2847.4 ± 1.5%	424.6	22.3 ± 0.2%	0.73
3.5	2487.3 ± 2.0%	424.6	22.8 ± 0.1%	0.83	7.5	2867.6 ± 1.7%	424.6	22.4 ± 0.3%	0.67
5.0	2661.0 ± 1.8%	424.6	22.2 ± 0.4%	0.77	10.0	2952.5 ± 1.6%	424.6	22.5 ± 0.2%	0.59
CTABr Micelles in 0.5 M NaBr									
1.4	2482.0 ± 1.0%	312.2	21.0 ± 0.3%	0.94	3.2	3162.5 ± 1.2%	312.2	21.5 ± 0.2%	0.86
2.0	2457.7 ± 1.2%	312.2	21.5 ± 0.3%	0.93	3.8	3683.6 ± 1.3%	312.2	21.6 ± 0.2%	0.83
2.6	2956.8 ± 1.2%	312.2	21.3 ± 0.2%	0.89	4.4	3677.2 ± 1.3%	312.2	21.7 ± 0.2%	0.81
CTABr Micelles in 1.0 M NaBr									
1.3	3810.5 ± 3.4%	324.0	22.8 ± 0.4%	0.93	2.6	5136.7 ± 2.7%	324.0	22.5 ± 0.3%	0.84
1.7	6196.5 ± 4.2%	324.0	22.7 ± 0.4%	0.87	3.2	6301.2 ± 2.4%	324.0	22.5 ± 0.3%	0.79
2.0	4794.3 ± 2.7%	324.0	22.4 ± 0.3%	0.87	3.8	6319.2 ± 2.4%	324.0	22.5 ± 0.3%	0.78
2.3	4912.7 ± 2.5%	324.0	22.6 ± 0.3%	0.85					

conclusion of the Monte Carlo simulation; that is, once interactions are accounted for, the micellar flexibility should not change with concentration.[28]

At present, it is not possible for us to determine the origin of the systematic disagreement when *b* is fixed in the PRISM fittings with the protocol proposed by Schurtenberger et al. It may result from the nature of this PRISM protocol: beyond a certain threshold of control parameters such as surfactant concentration, it is not realistic to expect that the scaling law of *S*(0), which is the cornerstone in this PRISM implementation, remains valid if it can be applied to render qualitatively correct scattering functions. The lack of successful model fitting indicates that this protocol is unable to describe the intermicellar interaction properly at least at high surfactant concentrations. Although it is generally believed that the apparent dependence of the flexibility on concentration is due to the disregard of intermicellar interactions, evidence collected from similar wormlike micellar systems reported by Kaler et al. but with completely different experimental approaches indeed suggests a different scenario.[29] In their studies, a combination of rheology and flow birefringence was used to

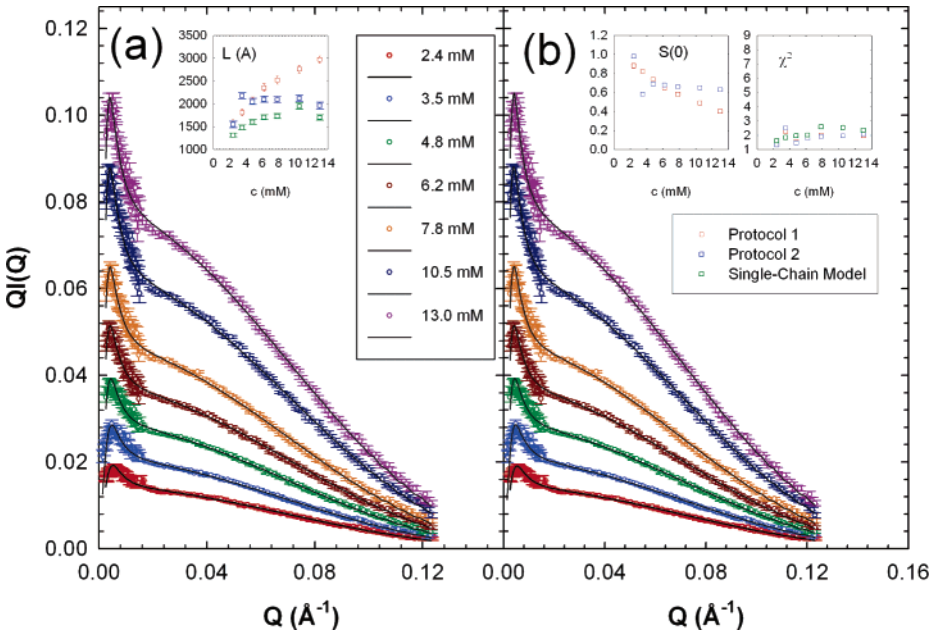

Figure 8. Comparison of fitting results presented in bending rod plots of the two different PRISM protocols. See the text for details.

Table 3. Fitted Parameters for Micelles in NaBr with the PRISM Model with Floating *b*

c(mM)	*L*(Å)	*b*(Å)	R_{CS}(Å)	*S*(0)	*c*(mM)	*L*(Å)	*b*(Å)	R_{CS}(Å)	*S*(0)
CPYBr Micelles in 0.25 M NaBr									
2.4	1582.2 ± 2.0%	395.5 ± 1.6%	21.0 ± 0.3%	0.88	7.8	2521.0 ± 2.2%	446.8 ± 1.1%	21.2 ± 0.2%	0.58
3.5	1812.1 ± 2.1%	401.3 ± 1.3%	21.2 ± 0.2%	0.82	10.5	2760.9 ± 2.3%	451.1 ± 1.1%	21.0 ± 0.1%	0.49
4.8	2073.6 ± 2.0%	439.0 ± 1.3%	21.2 ± 0.2%	0.74	13.0	2972.7 ± 2.4%	472.5 ± 1.2%	21.1 ± 0.1%	0.40
6.2	2355.7 ± 2.1%	451.7 ± 1.3%	21.2 ± 0.2%	0.65					
CPYBr Micelles in 0.5 M NaBr									
2.6	3514.6 ± 1.6%	351.5 ± 1.1%	21.2 ± 0.4%	0.82	6.2	4663.0 ± 1.7%	391.1 ± 0.9%	21.5 ± 0.3%	0.56
3.8	3818.7 ± 2.2%	356.3 ± 1.1%	21.4 ± 0.3%	0.74	7.8	5086.2 ± 1.8%	412.0 ± 0.8%	21.5 ± 0.2%	0.46
4.8	4044.7 ± 1.5%	358.8 ± 0.9%	21.3 ± 0.3%	0.68	10.0	5311.2 ± 1.7%	405.2 ± 0.8%	21.6 ± 0.2%	0.39
CPYBr Micelles in 0.8 M NaBr									
1.04	2100.4 ± 1.1%	252.5 ± 0.9%	19.2 ± 0.5%	0.96	2.5	3482.4 ± 2.8%	333.4 ± 1.2%	21.4 ± 0.4%	0.84
1.28	1949.2 ± 1.1%	265.6 ± 0.8%	19.2 ± 0.4%	0.96	3.1	3851.0 ± 2.9%	325.6 ± 1.0%	21.4 ± 0.3%	0.80
1.52	2178.7 ± 1.1%	268.1 ± 0.7%	19.6 ± 0.4%	0.94	3.12	3013.1 ± 1.7%	325.3 ± 0.6%	20.5 ± 0.2%	0.83
1.92	2513.7 ± 1.1%	283.9 ± 0.6%	19.9 ± 0.3%	0.91	4.0	4999.2 ± 4.1%	345.1 ± 0.9%	21.6 ± 0.3%	0.70
CTABr Micelles in 0.15 M NaBr									
2.0	930.6 ± 3.5%	835.6 ± 6.7%	21.3 ± 0.3%	0.83	5.0	1321.3 ± 1.8%	680.0 ± 1.9%	22.0 ± 0.2%	0.69
3.5	1130.4 ± 2.0%	735.9 ± 2.6%	21.8 ± 0.2%	0.76	7.5	1546.5 ± 1.7%	599.1 ± 1.5%	21.9 ± 0.2%	0.62
CTABr Micelles in 0.25 M NaBr									
2.4	2323.6 ± 2.3%	463.4 ± 1.6%	22.8 ± 0.1%	0.88	6.2	3579.5 ± 2.1%	538.5 ± 1.3%	22.3 ± 0.2%	0.62
3.5	2602.0 ± 2.4%	449.5 ± 1.8%	22.2 ± 0.4%	0.81	7.5	3501.0 ± 2.7%	512.1 ± 1.5%	22.4 ± 0.3%	0.57
5.0	2839.6 ± 2.2%	462.1 ± 1.6%	22.4 ± 0.3%	0.74	10.0	3866.0 ± 2.9%	527.5 ± 1.5%	22.5 ± 0.2%	0.46
CTABr Micelles in 0.5 M NaBr									
1.4	2607.9 ± 1.3%	330.4 ± 0.7%	21.0 ± 0.3%	0.93	3.2	3454.7 ± 2.2%	396.2 ± 0.7%	21.5 ± 0.2%	0.81
2.0	3168.9 ± 2.0%	367.9 ± 0.7%	21.5 ± 0.3%	0.89	3.8	4042.8 ± 2.8%	404.3 ± 0.6%	21.6 ± 0.2%	0.76
2.6	3968.1 ± 2.1%	373.1 ± 0.7%	21.3 ± 0.2%	0.84	4.4	4010.1 ± 2.8%	401.0 ± 0.6%	21.7 ± 0.2%	0.73
CTABr Micelles in 1.0 M NaBr									
1.3	3690.0 ± 3.8%	358.7 ± 1.9%	22.8 ± 0.4%	0.91	2.6	5784.8 ± 3.9%	421.4 ± 1.6%	22.5 ± 0.3%	0.77
1.7	6264.9 ± 4.4%	338.4 ± 1.2%	22.7 ± 0.4%	0.86	3.2	7625.3 ± 3.6%	398.6 ± 1.2%	22.5 ± 0.3%	0.71
2.0	5069.3 ± 3.4%	396.2 ± 1.5%	22.4 ± 0.3%	0.82	3.8	7762.3 ± 3.6%	414.6 ± 1.1%	22.5 ± 0.3%	0.69
2.3	5295.3 ± 3.1%	385.4 ± 1.4%	22.6 ± 0.3%	0.81					

determine the rigidity of the cetyltrimethylammonium tosylate (CTATos) and sodium dodecyl benzyl sulfonate (SDBS) worm-like micelles. In both cases, a clear increase in persistence length with surfactant concentration has been observed.

The fitted parameters of the single-chain model fitting and the PRISM model fitting with *b* as an optimization parameter are presented in Tables 1 and 3. It is important to note that for the PRISM fitting with floating *b*, like the Kuhn length obtained from the single-chain model fitting, a dependence on concentration remains observable but less evident. This may support the authenticity of the rigidity dependence on concentration if the validity of the PRISM approximation is justifiable under the current experimental conditions.

Comparison of PRISM Fittings of Protocols 1 and 2. A comparison between the experimental results of different CPyBr concentrations in 0.25 M NaBr solutions by two different protocols as mentioned before is given in Figure 8. Judging from the final χ^2, it is clearly shown that mathematically the two different

(29) Schubert, B. A.; Kaler, E. W.; Wagner, N. J. *Langmuir* **2003**, *19*, 4079.

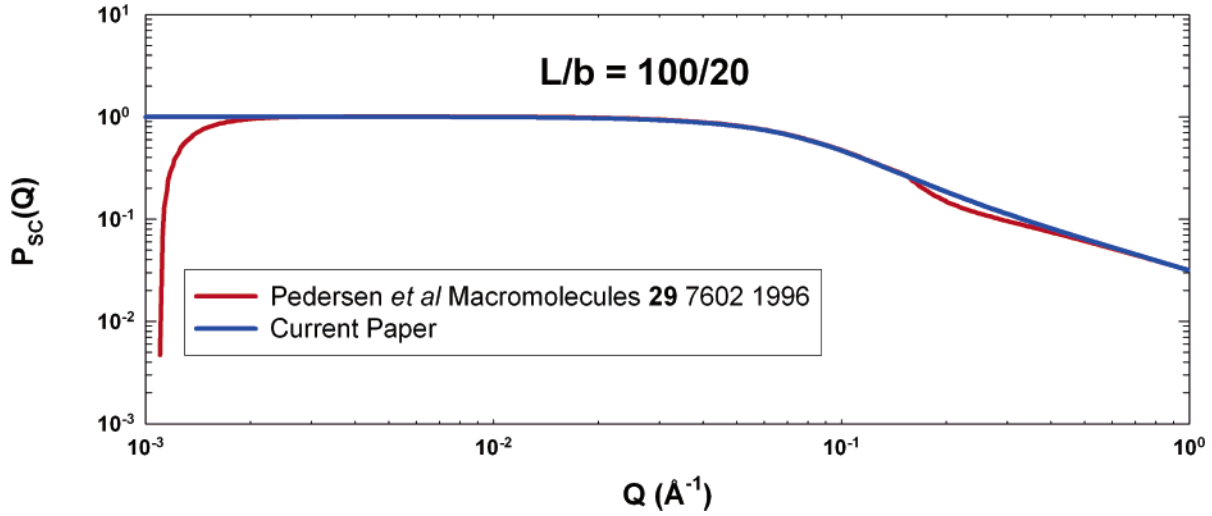

Figure 9. Comparison of the scattering functions of semiflexible chains with excluded volume effects. The red curve gives the model proposed by Schurtenberger et al,[8] and the blue line represents the same model after the modifications detailed in the text.

approaches are equally good. However, $S(0)$ obtained by two methods shows significant differences. Compared with the $S(0)$ obtained from Schurtenberger's protocol (protocol 1), upon increasing the surfactant concentration, the decay of $S(0)$ given by our proposed protocol (protocol 2) is less pronounced. The inconsistency may result from the following two reasons: First, protocol 2 is a more straightforward and simple approach than protocol 1. However, the experimental determination of the interaction parameter $S(0)$ via this expression relies heavily on the quality of the very low Q SANS intensity distribution. If the direct beam cannot be caught completely by the beam stop, then the values of important structural parameters such as contour length L obtained from this model fitting would be significantly overestimated. Therefore, $S(0)$ may be questionable. It is our conjecture that the apparent deviation of $S(0)$ for the 3.5 mM sample can be traced back to this experimental error.

Second, as pointed out in ref 12, although $S(0)$ derived from rigorous RGT calculations can be expressed as a function of surfactant concentration c, inconsistency was found when attempting to compare this scaling law of $S(0)$ with the results obtained from Monte Carlo simulation. A substitution of its associated coefficients was made to ensure its applicability.

The two different approaches give qualitatively reasonable results; that is, the interaction parameter $S(0)$ decreases as surfactant concentration c increases. The quantitative deviation may be due to a combination of the uncertainty of the absolute value of the very low Q SANS intensity distribution and the validity of the scaling law for the osmotic compressibility in the micellar systems that we studied.

Conclusions

We improved the parametrized scattering functions of the wormlike chain model proposed by Pedersen and Schurtenberger. As demonstrated in the Appendix and Figure 9, we found two vital numerical mistakes and modified the scattering function accordingly. It was found that this modified single-chain model fitting indeed gives satisfactory agreement with the experimental SANS data. In addition, it works well (see below) with interaction and a varying b. At constant salt concentration, the pyridinium headgroups confer more flexibility than trimethylammonium headgroups on the micelles. The hypothesis is that this is because of the geometry of the headgroups. Moreover, upon increasing the salt concentration, increasing micellar flexibility was observed as expected because of the screening of electronic repulsions. It also reveals a clear dependence of the Kuhn length on the surfactant concentration.

To incorporate intermicellar interactions, the PRISM model of protocol 1 was used for data analysis. The comparison of the two schemes used clearly shows that when b is fixed the quality of the model fitting deteriorates as surfactant concentration increases and therefore the unambiguous extraction of the structural information is questionable. However, if b is allowed to be optimized during the model fitting, then the agreement between the model and the SANS experimental data is significantly improved. As we know, before the present work there were no fully successful examples of allowing b to vary when interactions are included. The reason for this success may be from the repair of the single-chain scattering function, the reference system of PRISM. Compared with single-chain model fitting, a less remarkable dependence of micellar persistence length on surfactant concentration has been found.

We also showed that PRISM protocol with fixed b proposed by Schurtenberger et al. can be applied only to dilute solutions. The exact reason for the poor quality of the fits obtained at high concentration is not well understood. Kaler and co-workers did find b to depend on surfactant concentration in the systems of the CTATos and SDBS wormlike micelles using the techniques of rheology measurement and flow birefringence. Thus, the increase in intrinsic micellar rigidity as surfactant concentration increases in the CTABr and CPyBr systems may be real.

Furthermore, the two PRISM protocols that differ in how β, the interaction parameter, is obtained have been proved to be equally good in terms of model fitting. Our protocol is relatively simple mathematically. However, it is demonstrated that the quality of the low-Q SANS data has a significant effect on the fitting results.

Acknowledgment. We thank Dr. Zhibin Li for his assistance in performing the SANS experiments and in reducing the data. W.-R.C. thanks the National Science Foundation (CHE0316132) for financial support. A portion of this material is based upon work performed by L.J.M. while serving at the National Science Foundation. W.-R.C. gratefully thanks Dr. Steven. R. Kline of NCNR, NIST for many fruitful discussions. We acknowledge the support of the National Institute of Standards and Technology, U.S. Department of Commerce in providing the neutron research facilities supported under NSF agreement DMR-0454672.

Appendix

Modification of the Pedersen−Schurtenberger Single-Chain Scattering Function. In this article, we used the scattering function of semiflexible chains proposed by Pedersen and Schurtenberger. It is found that this computer model is statistically mechanically equivalent to real wormlike chain systems. Numerous experiments on different systems, such as polymeric liquids, wormlike micellar systems, and protein solutions, have demonstrated its robustness and wide applicability for obtaining essential configurational information.[18,30−34]

However, we do notice two unphysical errors occurring at certain L/b ratios in the scattering function. First, an unphysical negative value of $S(Q, L, b)$ is observed at low Q. It can be traced back to the coefficients associated with eq 13 of ref 8, shown identically in the second term of eq A.4, which are determined by Monte Carlo simulations. It is not possible for us to alter the coefficients to correct this error because we do not have access to the Monte Carlo simulation code. Our approach is to add an extra correction function $f_{corr}(Q)$ and rewrite the second terms of eq A.4 as

$$f_{corr}(Q)\, w(QR_G)[1.22(QR_G)^{-1/0.585} + 0.4288(QR_G)^{-2/0.585} - 1.651(QR_G)^{-3/0.585}] \quad \text{(A.1)}$$

where $f_{corr}(Q)$ is defined as

$$f_{corr}(Q) \equiv \begin{cases} 1 & \text{if } \dfrac{dS(Q, L, b)}{dQ} \le 0 \\ 0 & \text{if } \dfrac{dS(Q, L, b)}{dQ} > 0 \end{cases} \quad \text{(A.2)}$$

The result of our scattering function is shown as the blue curve in Figure 9.

Moreover, an artificial kink is observed in the intermediate-Q region, where the two asymptotic expressions of the scattering functions, eqs A.3 for high Q and eq A.4 for low Q, fit together.

$$S_1(Q, L, b) = \frac{a_1(Q, L, b)}{(Qb)^{4.95}} + \frac{a_2(Q, L, b)}{(Qb)^{5.29}} + \frac{\pi}{QL} \quad \text{(A.3)}$$

$$S_2(Q, L, b) = [1 - w(QR_G)]S_{Debye}(Q, L, b) + w(QR_G)[1.22(QR_G)^{-1/0.585} + 0.4288(QR_G)^{-2/0.585} - 1.651(QR_G)^{-3/0.585}] + \frac{C(n_b)}{n_b}\left\{\frac{4}{15} + \frac{7}{15u} - \left(\frac{11}{15} + \frac{7}{15u}\right) \times \exp[-u(Q, L, b)]\right\} \quad \text{(A.4)}$$

($w(QR_G)$ and $1 - w(QR_G)$ were mistakenly swapped in eq 13 of ref 8) where

$$S_{Debye}(Q, L, b) = \frac{2}{u(Q, L, b)}\{\exp[-u(Q, L, b)] + u(Q, L, b) - 1\}$$

$$u(Q, L, b) = \frac{Lb}{6}\left\{1 - \frac{3}{2n_b} + \frac{3}{2n_b^2} - \frac{3}{4n_b^3}[1 - \exp(-2n_b)]\right\}Q^2$$

$$n_b = \frac{L}{b}$$

$$w(x) = \frac{\{1 + \tanh[(x - 1.523)/0.1477]\}}{2}$$

$$\langle R_G^2 \rangle = \alpha(n_b)^2\frac{bL}{6}$$

$$u(Q, L, b) = \alpha(n_b)^2Q^2\frac{bL}{6}$$

$$\alpha(x) = \sqrt{\left[1 + \left(\frac{x}{3.12}\right)^2 + \left(\frac{x}{8.67}\right)^3\right]^{0.176/3}}$$

$$C(n_b) = \begin{cases} 3.06n_b^{-0.44} & \text{for } L > 10b \\ 1 & \text{for } L \le 10b \end{cases}$$

It is found from the mathematical expressions of $a_1(Q, L, b)$ and $a_2(Q, L, b)$ in eqs 23 and 24 of ref 8 (eq A.3 of the current paper). It is repaired by setting the two different functional forms and their first derivatives equal at the intersecting Q and calculating $a_1(Q, L, b)$ and $a_2(Q, L, b)$ analytically. The correct scattering curve is shown in Figure 9. Because of the complexity of $a_1(Q, L, b)$ and $a_2(Q, L, b)$, their exact mathematical expressions are given in the Supporting Information. The computer code, including the modified scattering function (written in MATLAB), used for our model fitting is available from L.J.M. (E-mail: lmagid@nsf.gov).

Supporting Information Available: Exact mathematical expressions for $a_1(Q, L, b)$ and $a_2(Q, L, b)$. This material is available free of charge via the Internet at http://pubs.acs.org.

LA0530440

(30) Jerke, G.; Pedersen, J. S.; Egelhaaf, S. U.; Schurtenberger, P. *Langmuir* **1998**, *14*, 6013.
(31) Magid, L. J.; Han, Z.; Li, Z.; Butler, P. D. *J. Phys. Chem. B* **2000**, *104*, 6717.
(32) Magid, L. J.; Li, Z.; Butler, P. D. *Langmuir* **2000**, *16*, 10028.
(33) Russo, D.; Durand, D.; Desmadril, M.; Calmeltes, P. *Physica B* **2000**, *276*, 520.
(34) Egelhaaf, S. U.; van Swieten, E.; Bosma, T.; de Boef, E.; van Dijk, A. A.; Robillard, G. T. *Biopolymers* **2003**, *69*, 311.